# Buoyancy driven dissolution of inclined blocks: Erosion rate and pattern formation
# Supplemental material - Raw data

Caroline Cohen, Michael Berhanu, Julien Derr, and Sylvain Courrech du Pont*
*Laboratoire Matières et Systèmes Complexes*
*Université de Paris, CNRS*
*Bâtiment Condorcet, 10 rue Alice Domon et Léonie Duquet,*
*75205 Paris cedex 13, France*

We suppose a linear relationship between concentration $C$ and density $\rho$ of solutions :

$$C = \frac{\rho - \rho_0}{\rho_{\rm sat} - \rho_0} C_{\rm sat}, \tag{1}$$

where $\rho_0 = \rho(C = 0)$ and where $\rho_{\rm sat}$ and $C_{\rm sat}$ are the density and the saturation concentration, respectively.

For the calculations of the scaling laws for the experiments with salt, we use the measured values $\rho_0 = 997.12$ kg.m$^{-3}$, $\rho_{\rm sat} = 1197.3$ kg.m$^{-3}$ and $\rho_{\rm s} = 2348$ kg.m$^{-3}$. We calculate $C_{\rm sat} = 317.25$ kg.m$^{-3}$ from the tabulated value of the solubility $S = 359.45$ kg.m$^{-3}$ ($C_{\rm sat} = S\rho_{\rm sat}/(S + \rho_0)$). We use $D = 1.59 \times 10^{-9}$ m$^2$.s$^{-1}$ for the coefficient of diffusion of the saturated brine [1]. Figure 1 shows our measurements of the viscosity of salt solutions as a function of their density. Raw data of experiments are listed in table I. Figure 2 shows the dependency of the receding velocity on the inclination angle and the density of the outer bath. Figure 3 shows the dependency of the wavelength of incipient longitudinal stripes on the density of the outer bath.
Alkattan *et al.* measured the dissolution velocity set by the chemical kinetic of salt in water. They found $\alpha \simeq 5 \times 10^{-4}$ m/s [2]. Thus, the characteristic thickness over which the dissolution is limited by diffusion is $D/\alpha \simeq 3.2 \times 10^{-6}$ mm. This is much smaller than the values of wavelengths we measure in our experiments, which justifies the diffusion limited approximation, *i.e.* to reduce the value of the concentration at the interface to the one of the saturation concentration.

For the experiment with plaster, the solution was tap water and the inclinatination was $\theta = 52$ deg. We measured $\lambda_{\rm s} = 2.25 \pm 0.4$ mm and $-\dot{h} = 2.97 \times 10^{-6} \pm 6.5 \times 10^{-7}$ mm/s. We use $D = 1 \times 10^{-9}$ m$^2$.s$^{-1}$ (from tabulations, [3]), $\rho_{\rm sat} - \rho_0 = 1.8$ kg.m$^{-3}$ (measured), $C_{\rm sat} = 2.04$ kg.m$^{-3}$ (tabulated), $\eta_{\rm f} = 0.89 \times 10^{-3}$ Pa.s (pure water), and $\rho_{\rm s} = 1859$ kg.m$^{-3}$ (measured) for the calculation of the scaling law.
Colombani and Bert measured the dissolution velocity set by the chemical kinetic of gypsum in water, they found $\alpha \simeq 2.7 \times 10^{-6}$ m/s [3]. Thus, the characteristic thickness over which the dissolution is limited by diffusion is $D/\alpha \simeq 0.37$ mm. It is (only) 6 times smaller than the wavelength value we measured, which barely justifies the dissolution limited approximation.

For the calculations of scaling laws for experiments with caramel, we use the measured values $\rho_0 = 997$ kg.m$^{-3}$, $\rho_{\rm sat} = 1450$ kg.m$^{-3}$and $\rho_{\rm s} = 1540$ kg.m$^{-3}$. $C_{\rm sat} = 968.26$ kg.m$^{-3}$ is calculated from the measured value of $\rho_{\rm sat}$ and the tabulated value of the sucrose solubility $S = 2004$ kg.m$^{-3}$ ($C_{\rm sat} = S\rho_{\rm sat}/(S + \rho_0)$). Figure 4 shows our measurement of the viscosity of caramel solutions as a function of their density. We estimate the coefficient of diffusion of the saturated solution $D = 1.34 \times 10^{-12}$ m$^2$/s from the tabulated value at zero concentration ($5.2 \times 10^{-8}$ m$^2$/s) that we extrapolate to the saturated solution using the Stokes-Einstein relation. The error may be large for this value. This would affect the comparison between experiments with caramel and other dissolving materials but it should not affect the scaling laws when comparing the different caramel experiments with each other. We have chosen to use the value of the saturated solution for the diffusion coefficient whatever the concentration of the bath solution. Raw data are listed in tables II, III, IV and V. Figure 5 shows the dependency of the receding velocity on the inclination angle and the density of the outer bath. Figure 6 shows the dependency of the wavelength of incipient longitudinal stripes and of the characteristic time to observe them on the inclination angle and the density of the outer bath.
An easy way of estimating a lower bound of the characteristic dissolution velocity $\alpha$ of a material consists in measuring the rate of dissolution of a body of this material in a water flow as fast as possible. Thereby, the thickness of the

* sylvain.courrech@univ-paris-diderot.fr

| $\rho_b$ (kg.m$^{-3}$) | $\theta$ (deg) | $-\dot{h}$ (mm/s) | $\lambda_s$ (mm) | $C_b$ (kg.m$^{-3}$) | $C_f$ (kg.m$^{-3}$) | $\eta_f$ ($\times 10^{-3}$ Pa.s) |
|---|---|---|---|---|---|---|
| 997.12 | 6 | $6.35 \times 10^{-3} \pm 2 \times 10^{-4}$ | | 0 | 158.63 | 1.23 |
| 997.12 | 11.5 | $5.18 \times 10^{-3} \pm 5 \times 10^{-4}$ | | 0 | 158.63 | 1.23 |
| 997.12 | 21.4 | $5.13 \times 10^{-3} \pm 1 \times 10^{-4}$ | | 0 | 158.63 | 1.23 |
| 997.12 | 29.6 | $5.67 \times 10^{-3} \pm 1 \times 10^{-4}$ | | 0 | 158.63 | 1.23 |
| 997.12 | 45.4 | $4.2 \times 10^{-3} \pm 4 \times 10^{-4}$ | | 0 | 158.63 | 1.23 |
| 997.12 | 60.1 | $4.21 \times 10^{-3} \pm 3 \times 10^{-4}$ | | 0 | 158.63 | 1.23 |
| 997.12 | 70.8 | $3.5 \times 10^{-3} \pm 1.6 \times 10^{-4}$ | | 0 | 158.63 | 1.23 |
| 997.12 | 74.5 | $3 \times 10^{-3} \pm 4 \times 10^{-4}$ | | 0 | 158.63 | 1.23 |
| 997.12 | 79.8 | $3.23 \times 10^{-3} \pm 3.5 \times 10^{-4}$ | | 0 | 158.63 | 1.23 |
| 997.12 | 86.8 | $2.12 \times 10^{-3} \pm 2.4 \times 10^{-4}$ | | 0 | 158.63 | 1.23 |
| 999.8 | 30 | $5.67 \times 10^{-3} \pm 1.1 \times 10^{-4}$ | | 4.25 | 160.75 | 1.24 |
| 1025 | 30 | $3.59 \times 10^{-3} \pm 1.8 \times 10^{-4}$ | | 44.18 | 180.72 | 1.31 |
| 1065 | 30 | $2.08 \times 10^{-3} \pm 1 \times 10^{-4}$ | | 107.58 | 212.41 | 1.43 |
| 1108 | 30 | $1.29 \times 10^{-3} \pm 1.9 \times 10^{-4}$ | | 175.73 | 246.49 | 1.58 |
| 1152.6 | 30 | $3.85 \times 10^{-4} \pm 7.7 \times 10^{-5}$ | | 246.41 | 281.83 | 1.76 |
| 1178 | 30 | $1.53 \times 10^{-4} \pm 8.3 \times 10^{-6}$ | | 286.66 | 301.96 | 1.87 |
| 1188.4 | 30 | $1.65 \times 10^{-5} \pm 2 \times 10^{-6}$ | | 303.15 | 310.2 | 1.92 |
| 1197 | 0 | $2.56 \times 10^{-6} \pm 5 \times 10^{-7}$ | | 316.78 | 317.01 | 1.96 |
| 1179.6 | 82.7 | $8.37 \times 10^{-5} \pm 5 \times 10^{-6}$ | | 289.2 | 303.2 | 1.88 |
| 1179 | 5 | $1.27 \times 10^{-4}$ | | 288.25 | 302.75 | 1.88 |
| 1172.7 | 84.2 | $1.32 \times 10^{-4} \pm 5 \times 10^{-6}$ | | 278.26 | 297.76 | 1.85 |
| 1171.9 | 29.3 | $2.3 \times 10^{-4} \pm 5 \times 10^{-5}$ | | 277 | 297.12 | 1.84 |
| 1105.8 | 69.8 | $1.02 \times 10^{-3} \pm 5 \times 10^{-5}$ | | 172.24 | 244.74 | 1.57 |
| 1020.15 | 80.3 | $2.24 \times 10^{-3} \pm 1 \times 10^{-4}$ | | 36.5 | 176.87 | 1.3 |
| 1012.3 | 21 | $3.89 \times 10^{-3} \pm 1 \times 10^{-4}$ | $0.56 \pm 0.2$ | 24.06 | 170.65 | 1.27 |
| 1182.4 | 45 | | $1.55 \pm 0.3$ | 293.64 | 305.4 | 1.89 |
| 1192.6 | 45 | | $2.4 \pm 0.4$ | 309.8 | 313.53 | 1.94 |
| 1192.2 | 82 | | $3.2 \pm 0.7$ | 309.17 | 313.21 | 1.94 |
| 997 | 70 | | $0.61 \pm 0.3$ | 0 | 158.53 | 1.23 |
| 1105.6 | 70 | | $0.8 \pm 0.1$ | 171.92 | 244.59 | 1.57 |
| 1119.2 | 70 | | $0.915 \pm 0.1$ | 193.48 | 255.36 | 1.62 |
| 1134.8 | 70 | | $1.09 \pm 0.05$ | 218.2 | 267.72 | 1.69 |
| 1164.4 | 70 | | $1.21 \pm 0.15$ | 265.11 | 291.18 | 1.81 |

TABLE I. Raw data of the receding velocity $\dot{h}$ and of the first observed wavelength $\lambda_s$ of the longitudinal stripes at the bottom interface of inclined blocks of salt into saline solutions of various densities. We measure the density $\rho_b$ of the solution and the inclination $\theta$ of the block. Measurement uncertainties are $2-3\,\mathrm{kg.m^{-3}}$ for $\rho_b$ and $1-2$ deg for $\theta$. We calculate the concentration $C_b$ of the solution from the density $\rho_b$. The characteristic concentration $C_f$ in the solute layer is taken halfway between the concentration of the solution and the saturation concentration $C_{sat} = 317\,\mathrm{kg.m^{-3}}$. $C_{sat}$ is calculated from the measured density of the saturated brine $\rho_{sat} = 1197.3\,\mathrm{kg.m^{-3}}$ and the tabulated value of the solubilty (359.45 g of salt for one liter of water). The characteristic viscosity $\eta_f$ inside the solute layer is calculated from the characteristic density $\rho_f$ (fig. 1). Experiments were done at room temperature ($\sim 22°$C).

solute boundary layer is very thin and the system approaches the regime where the dissolution is limited by the chemical kinetic. Doing so with a magnetic stirrer, we found $5 \times 10^{-6}$ m/s as a rough lower bound for $\alpha$. Taking the value of the coefficient of diffusion at zero concentration $D = 5.2 \times 10^{-8}$ m$^2$/s gives an upper bound value of $D/\alpha$ of $1 \times 10^{-2}$ m which is larger than the wavelengths we observe. Taking the value of the coefficient of diffusion at the saturation concentration $D = 1.34 \times 10^{-12}$ m$^2$/s gives an upper bound value of $D/\alpha$ of about $2 \times 10^{-7}$ m, which is much smaller than the values of wavelengths we measure on caramel blocks.


[1] V. Vitagliano and P. A. Lyons, Diffusion coefficients for aqueous solutions of sodium chloride and barium chloride, Journal of the American Chemical Society **78**, 1549 (1956).

[2] M. Alkattan, E. H. Oelkers, J.-L. Dandurand, and J. Schott, Experimental studies of halite dissolution kinetics, 1 the effect of saturation state and the presence of trace metals, Chemical Geology **137**, 201 (1997).

[3] J. Colombani and J. Bert, Holographic interferometry study of the dissolution and diffusion of gypsum in water, Geochimica et cosmochimica acta **71**, 1913 (2007).

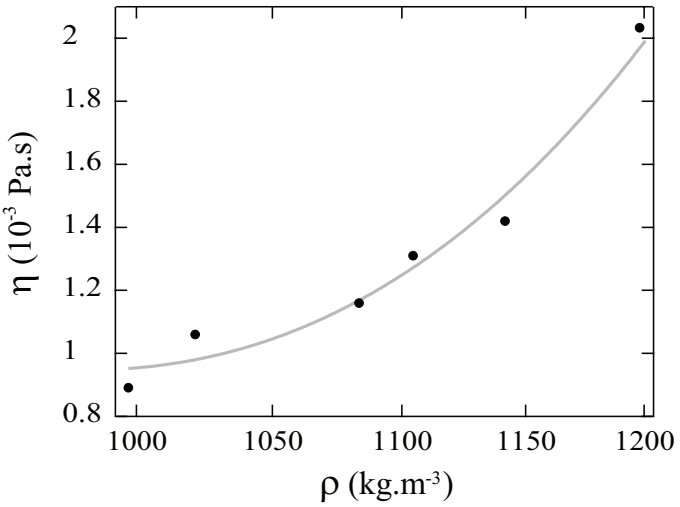


FIG. 1. Dynamic viscosity $\eta$ of table salt solutions as a function of the solution density $\rho$ at $T = 22°C$. The grey curve is the polynomial fit we use to calculate the viscosity: $y = 22.471 - 0.043753x + (2.2236 \times 10^{-6})x^2$.

| $\theta$ (deg) | $-\dot{h}$ ($\times 10^{-3}$ mm/s) |
|---|---|
| 0.5 | $3.47 \pm 0.03$ |
| 20 | 3.64 ” |
| 43 | 2.92 ” |
| 73 | 2.89 ” |
| 88 | 1.13 ” |
| 31 | 3 ” |
| 33 | 3.06 ” |
| 38.5 | 3.17 ” |
| 51 | 2.75 ” |
| 51 | 3.39 ” |
| 62 | 2.78 ” |
| 63 | 2.28 ” |
| 66 | 2.67 ” |
| 69 | 2.17 ” |
| 74 | 1.86 ” |
| 78 | 2.08 ” |
| 82 | 1.81 ” |
| 88 | 1.08 ” |

TABLE II. Raw data of the receding velocity $\dot{h}$ at the bottom interface of caramel blocks into water with different inclination angles $\theta$. The concentration of the outer solution is zero. For the calculations we take the density of the solution $\rho_{\rm b} = 997.3\,{\rm kg.m^3}$ and the characteristic concentration and viscosity inside the soluter layer to be $C_{\rm f} = 484.13\,{\rm kg.m^3}$ and $\eta_{\rm f} = 1.46 \times 10^{-2}\,{\rm Pa.s}$. The characteristic viscosity $\eta_{\rm f}$ inside the solute layer is calculated from the characteristic density $\rho_{\rm f}$ (fig. 4).

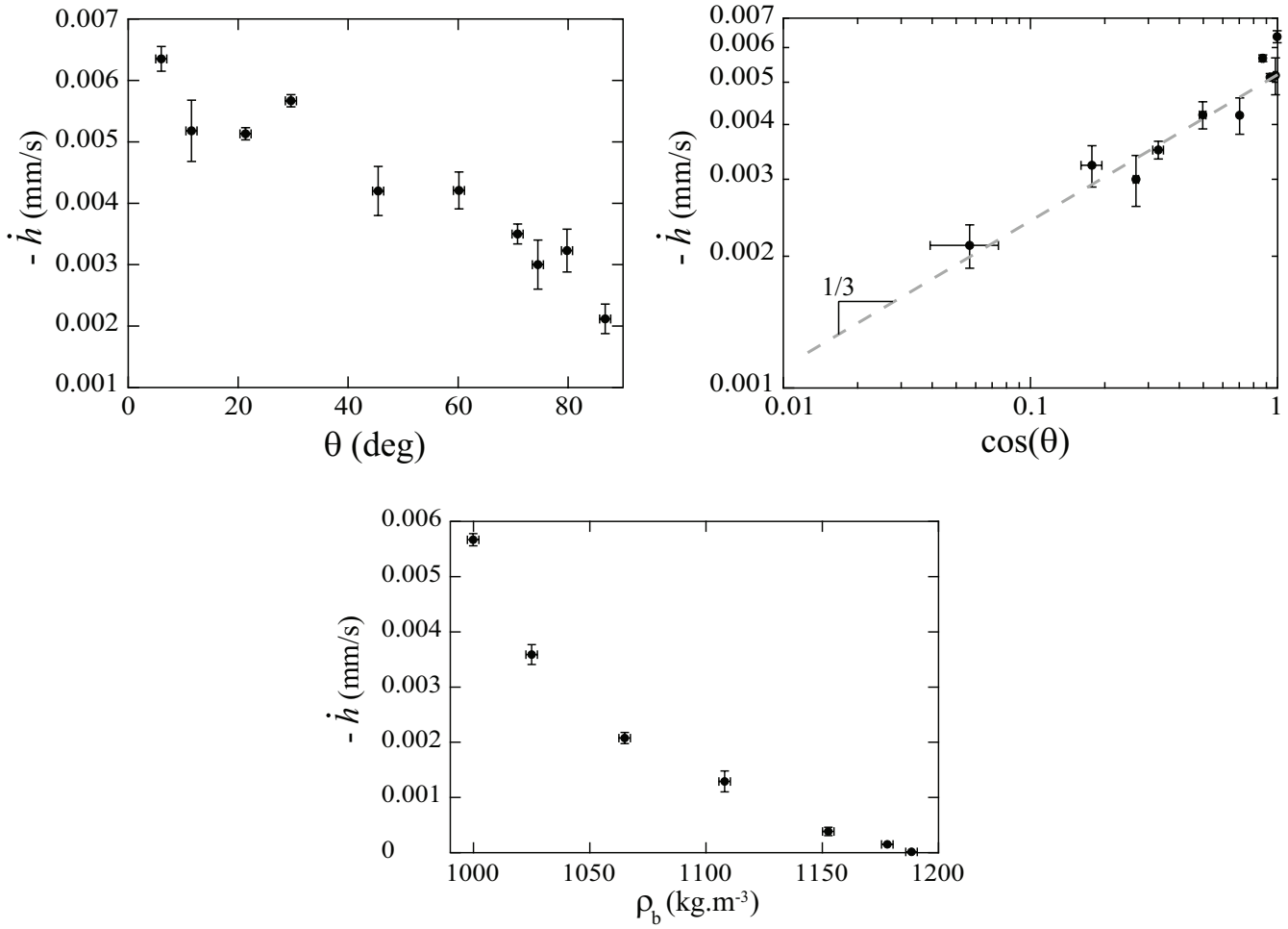


FIG. 2. Receding velocity $\dot{h}$ of the bottom interface of salt blocks in tap water as a function of the inclination angle $\theta$ (top left), as a function of $\cos(\theta)$ with logarithmic axes (top right) and inclined of 30 deg as a function of the density $\rho_b$ of the saline solution of the outer bath (bottom).

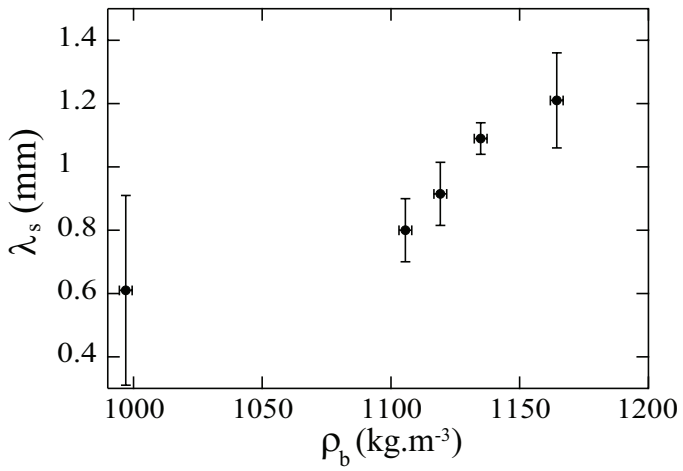


FIG. 3. Top: First observed wavelength $\lambda_s$ of longitudinal patterns as a function of the density of the saline solution of the outer bath. The inclination angle of blocks is $\theta = 30$ deg.

| $\rho_b$ (kg.m$^{-3}$) | $\theta$ (deg) | $-\dot{h}$ ($\times 10^{-3}$ mm/s) | $C_b$ (kg.m$^{-3}$) | $C_f$ (kg.m$^{-3}$) | $\eta_f$ (Pa.s) |
|---|---|---|---|---|---|
| 1000 | 73 | 1.79 | 0 | 484.07 | 0.0149 |
| 1000 | 73 | 2.89 | 0 | 484.07 | 0.0149 |
| 1000 | 75 | 2.66 | 0 | 484.07 | 0.0149 |
| 1001 | 73 | 1.39 | 0 | 484.1 | 0.015 |
| 1100 | 73 | 0.836 | 219.66 | 593.961 | 0.0348 |
| 1190 | 73 | 0.364 | 412.16 | 690.209 | 0.116 |
| 1250 | 73 | 0.166 | 540.49 | 754.375 | 0.442 |
| 1310 | 73 | 0.0706 | 668.82 | 818.541 | 1.78 |
| 1320 | 73 | 0.0617 | 690.21 | 829.235 | 2.38 |
| 1050 | 73 | 0.973 | 112.72 | 540.489 | 0.0218 |
| 1100 | 75 | 0.927 | 219.66 | 593.961 | 0.0348 |
| 1150 | 75 | 0.822 | 326.60 | 647.432 | 0.0627 |
| 1200 | 75 | 0.619 | 433.55 | 700.904 | 0.137 |
| 1250 | 75 | 0.25 | 540.49 | 754.375 | 0.442 |
| 1300 | 75 | 0.151 | 647.43 | 807.846 | 1.41 |
| 1320 | 75 | 0.151 | 690.21 | 829.235 | 2.38 |
| 1403 | 75 | 0.00278 | 867.73 | 917.997 | 20.07 |

TABLE III. Raw data of the receding velocity $\dot{h}$ at the bottom interface of inclined caramel blocks into sucrose-water solutions. Last line corresponds to an inclined caramel block into a water-caramel solution. The uncertainties are about 20% of the measured values. The characteristic viscosity $\eta_f$ inside the solute layer is calculated from the characteristic density $\rho_f$ (fig. 4).

| $\rho_b$ (kg.m$^{-3}$) | $\theta$ (deg) | $\lambda_s$ (mm) | $T_s$ (s) | $C_b$ (kg.m$^{-3}$) | $C_f$ (kg.m$^{-3}$) | $\eta_f$ (Pa.s) |
|---|---|---|---|---|---|---|
| 1432 | 73 | | $321300 \pm 100$ | 929.76 | 949.01 | 32.38 |
| 1410 | 73 | | $143700 \pm 100$ | 882.71 | 925.48 | 22.78 |
| 1403 | 73 | $4.45 \pm 0.8$ | | 867.73 | 918 | 20.07 |
| 1356 | 73 | $3.2 \pm 0.4$ | | 767.21 | 867.73 | 5.8 |
| 1303 | 70 | $1.57 \pm 0.29$ | $1590 \pm 10$ | 653.85 | 811.06 | 1.5 |
| 1274 | 71 | $1.26 \pm 0.2$ | $390 \pm 10$ | 591.82 | 780.04 | 0.765 |
| 1229 | 75 | $0.99 \pm 0.44$ | $150 \pm 10$ | 495.57 | 731.92 | 0.273 |
| 1155 | 75 | $0.63 \pm 0.2$ | $30 \pm 10$ | 337.3 | 652.78 | 0.0669 |
| 1108 | 72 | $0.52 \pm 0.15$ | $20 \pm 10$ | 236.77 | 602.52 | 0.0381 |
| 1075 | 72 | $0.55 \pm 0.18$ | $15 \pm 5$ | 166.19 | 567.23 | 0.0268 |
| 1041 | 70 | $0.45 \pm 0.24$ | $10 \pm 5$ | 93.47 | 530.86 | 0.0203 |
| 1006 | 72 | $0.41 \pm 0.16$ | $1 \pm 1$ | 18.61 | 493.44 | 0.0155 |
| 1000 | 75 | $0.44 \pm 0.17$ | $1 \pm 1$ | 0 | 484.07 | 0.0149 |
| 1000 | 60 | $0.4 \pm 0.2$ | | 0 | 484.07 | 0.0149 |

TABLE IV. Raw data of the first observed wavelength $\lambda_s$ of the longitudinal stripes and the characteristic time $T_s$ to observe them on inclined caramel blocks into water-caramel solutions of various densities $\rho_b$. We measure the density $\rho_b$ of the solution and the inclination $\theta$ of the block. We calculate the concentration $C_b$ of the solution from the density $\rho_b$. The characteristic concentration $C_f$ in the solute layer is taken halfway between the concentration of the solution and the saturation concentration $C_{sat} = 968.13\,\mathrm{kg.m^{-3}}$. $C_{sat}$ is calculated from the measured density of the saturated solution $\rho_{sat} = 1450\,\mathrm{kg.m^{-3}}$. Experiments were done at room temperature ($\sim 22°\mathrm{C}$). The characteristic viscosity $\eta_f$ inside the solute layer is calculated from the characteristic density $\rho_f$ (fig. 4).

| $\rho_b$ (kg.m$^{-3}$) | $\theta$ (deg) | $\lambda_s$ (mm) | $T_s$ (s) | $C_b$ (kg.m$^{-3}$) | $C_f$ (kg.m$^{-3}$) | $\eta_f$ (Pa.s) |
|---|---|---|---|---|---|---|
| 1000 | 74 | $0.39 \pm 0.14$ | | 0 | 484.07 | 0.0149 |
| 1000 | 75 | $0.38 \pm 0.18$ | | 0 | 484.07 | 0.0149 |
| 1000 | 76 | $0.44 \pm 0.24$ | $1 \pm 1$ | 0 | 484.07 | 0.0149 |
| 1320 | 75 | $2.1 \pm 0.4$ | $1800 \pm 100$ | 690.21 | 829.24 | 2.38 |
| 1230 | 74 | $0.76 \pm 0.25$ | | 497.71 | 732.99 | 0.279 |
| 1295 | 75 | $1.54 \pm 0.76$ $420 \pm 10$ | 636.74 | 802.5 | 1.26 | |
| 1140 | 75 | $0.51 \pm 0.25$ | | 305.22 | 636.74 | 0.0559 |
| 1040 | 75 | $0.4 \pm 0.24$ | $8 \pm 2$ | 91.33 | 529.8 | 0.0201 |
| 1100 | 75 | $0.59 \pm 0.23$ | $8 \pm 2$ | 219.66 | 593.96 | 0.0348 |
| 1080 | 75 | $0.48 \pm 0.2$ | | 176.88 | 572.57 | 0.0281 |
| 1220 | 73 | $0.71 \pm 0.32$ | | 476.32 | 722.29 | 0.218 |
| 1275 | 74 | $1.1 \pm 0.4$ | $270 \pm 10$ | 593.96 | 781.11 | 0.784 |
| 1300 | 76 | $1.64 \pm 0.56$ | $510 \pm 10$ | 647.43 | 807.85 | 1.41 |
| 1200 | 75 | $0.85 \pm 0.46$ | | 433.55 | 700.9 | 0.137 |
| 1210 | 73 | $0.64 \pm 0.43$ | | 454.94 | 711.6 | 0.17 |
| 1285 | 75 | $1.275 \pm 0.43$ | $400 \pm 20$ | 615.35 | 791.81 | 0.998 |
| 1197 | 75 | $0.79 \pm 0.31$ | | 427.13 | 697.7 | 0.13 |
| 1235 | 76 | $0.73 \pm 0.25$ | | 508.41 | 738.33 | 0.315 |
| 1249 | 75 | $0.91 \pm 0.51$ | | 538.35 | 753.31 | 0.43 |
| 1310 | 76 | $1.84 \pm 0.74$ | $1650 \pm 20$ | 668.82 | 818.54 | 1.78 |
| 1305 | 74 | $1.64 \pm 0.46$ | $960 \pm 20$ | 658.13 | 813.19 | 1.57 |
| 1240 | 75 | $0.97 \pm 0.51$ | $115 \pm 10$ | 519.1 | 743.68 | 0.354 |
| 1255 | 75 | $0.935 \pm 0.33$ | | 551.183 | 759.72 | 0.49 |
| 1319 | 76 | $1.93 \pm 0.57$ | | 688.07 | 828.17 | 2.31 |
| 1280 | 77 | $1.17 \pm 0.43$ | $320 \pm 10$ | 604.66 | 786.46 | 0.885 |
| 1260 | 76 | $1.09 \pm 0.51$ | $150 \pm 20$ | 561.88 | 765.07 | 0.547 |
| 1215 | 77 | $0.69 \pm 0.39$ | $85 \pm 5$ | 465.63 | 716.95 | 0.192 |
| 1150 | 85 | $0.77 \pm 0.41$ | $160 \pm 10$ | 326.6 | 647.43 | 0.0627 |
| 1150 | 80 | $0.66 \pm 0.29$ | $65 \pm 5$ | 326.6 | 647.43 | 0.0627 |
| 1150 | 75 | $0.62 \pm 0.25$ | $45 \pm 5$ | 326.6 | 647.43 | 0.0627 |
| 1150 | 60 | $0.49 \pm 0.15$ | $24 \pm 4$ | 326.6 | 647.43 | 0.0627 |
| 1150 | 45 | $0.45 \pm 0.28$ | $18 \pm 2$ | 326.6 | 647.43 | 0.0627 |

TABLE V. Raw data of the first observed wavelength $\lambda_s$ of the longitudinal stripes and the characteristic time $T_s$ to observe them on inclined caramel blocks into sucrose solutions of various densities $\rho_b$. We measure the density $\rho_b$ of the solution and the inclination $\theta$ of the block. We calculate the concentration $C_b$ of the solution from the density $\rho_b$. The characteristic concentration $C_f$ in the solute layer is taken halfway between the concentration of the solution and the saturation concentration $C_{sat} = 968.13\,\mathrm{kg.m^{-3}}$. $C_{sat}$ is calculated from the measured density of the saturated solution $\rho_{sat} = 1450\,\mathrm{kg.m^{-3}}$. Experiments were done at room temperature ($\sim 22°\mathrm{C}$). The characteristic viscosity $\eta_f$ inside the solute layer is calculated from the characteristic density $\rho_f$ (fig. 4).

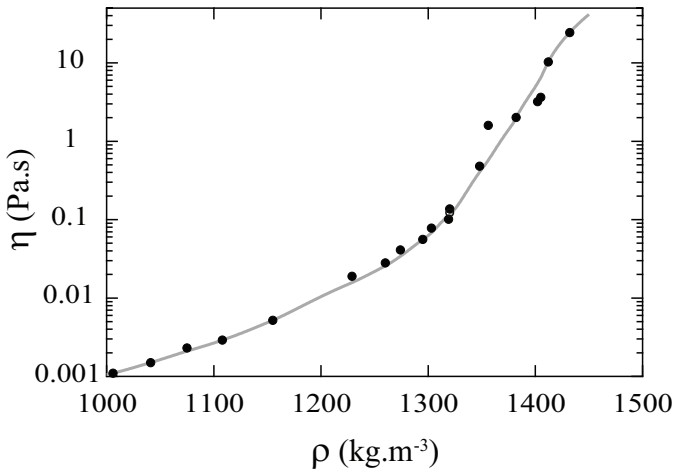


FIG. 4. Dynamic viscosity $\eta$ of caramel solutions as a function of the solution density $\rho$ at $T = 21°C$. The empty symbol ($\rho = 1320$ kg.m$^{-3}$) is a measurement for a sucrose solution. The grey curve is a polynomial fit used to calculate $\eta_f$.

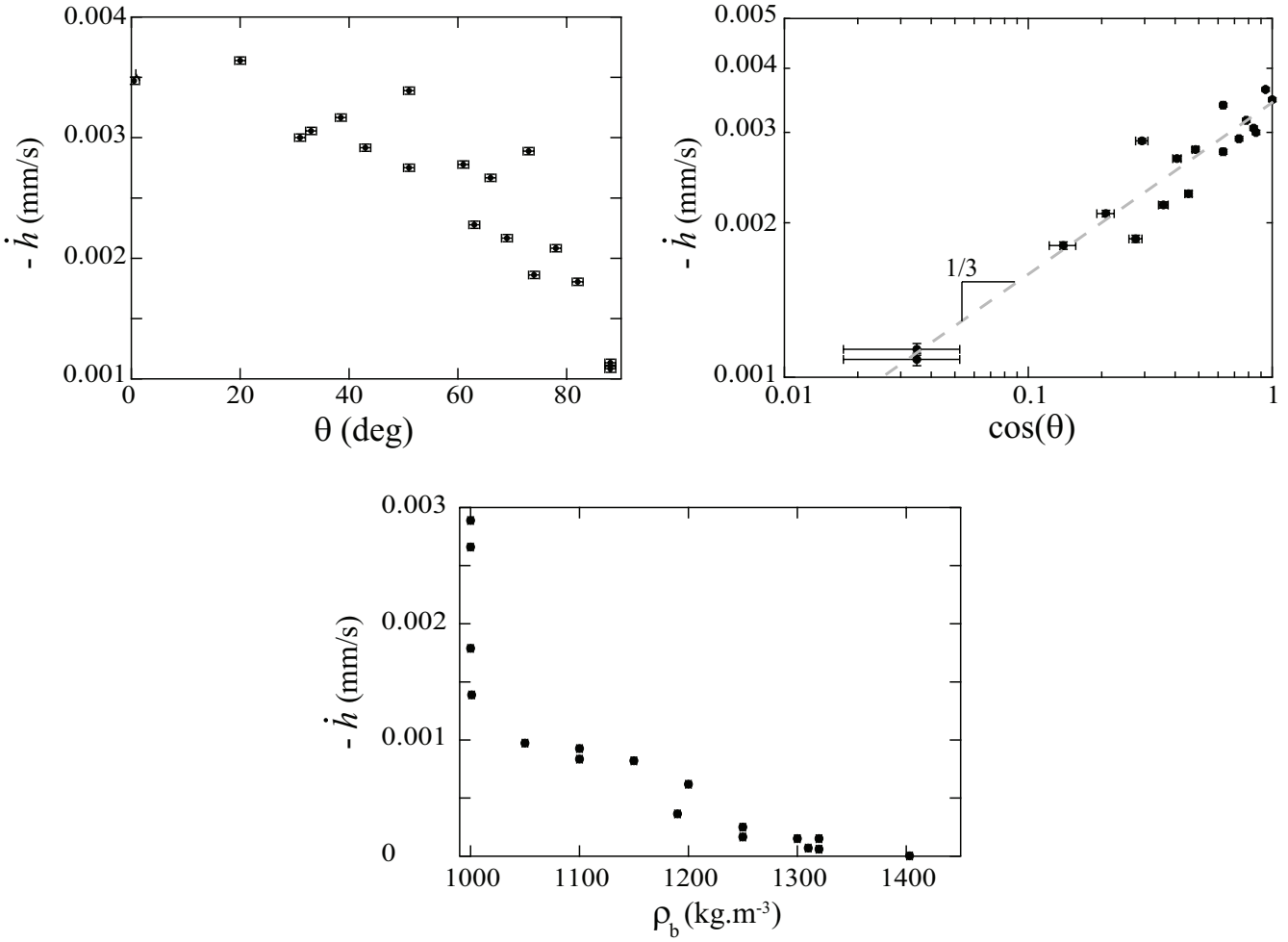


FIG. 5. Receding velocity $\dot{h}$ of the bottom interface of caramel blocks in tap water as a function of the inclination angle $\theta$ (top left), as a function of $\cos(\theta)$ with logarithmic axes (top right) and inclined of an angle ranging between 73 and 76 deg as a function of the density $\rho_b$ of the sucrose - water solution of the outer bath (bottom).

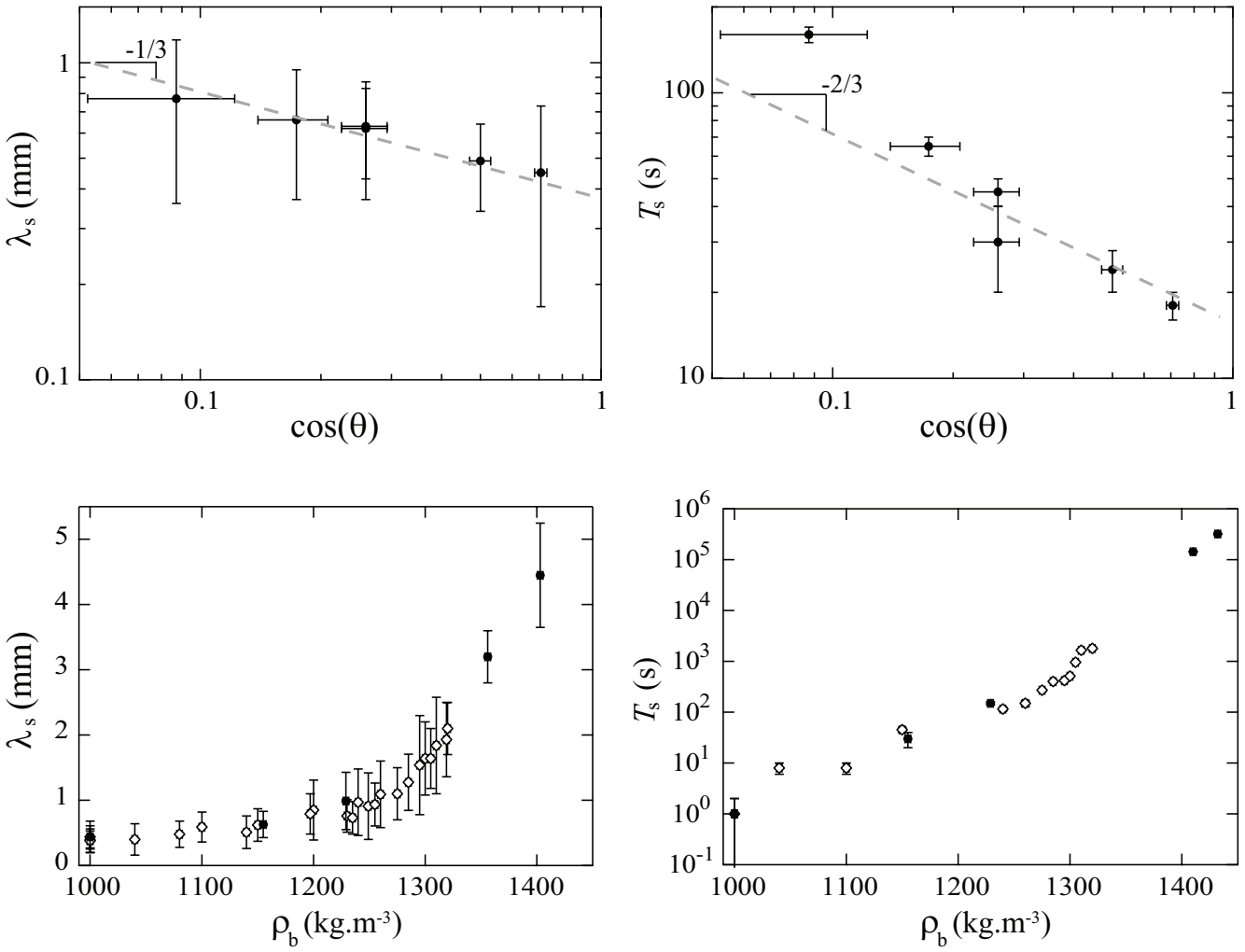


FIG. 6. Top: First observed wavelength $\lambda_s$ of longitudinal patterns (left) and characteristic time $T_s$ to observe them (right) as a function of the inclination $\cos(\theta)$ with logarithmic axes. The density of the sucrose - water solution is $\rho_b = 1150$ kg.m$^{-3}$. Bottom: First observed wavelength $\lambda_s$ of longitudinal patterns (left) and characteristic time $T_s$ to observe them (right) as a function of the density $\rho_b$ of the outer bath. The inclination angle ranges between 73 and 76 deg. The outer bath is either a caramel - water solution (plain circles) or a sucrose - water solution (empty diamonds).